Signal Processing 139 (2017) 156–164

Contents lists available at ScienceDirect

Signal Processing

journal homepage: www.elsevier.com/locate/sigpro

MUSIC-like direction of arrival estimation based on virtual array transformation

Feng-Gang Yan[a,b], Xue-Wei Yan[a], Jun Shi[c,*], Jun Wang[a], Shuai Liu[a], Ming Jin[a], Yi Shen[b]

[a] School of information and Electrical Engineering, Harbin Institute of Technology at Weihai, Weihai, 264209, China
[b] School of Astronautics, Harbin Institute of Technology, Harbin, 150001, China
[c] Communication Research Center, Harbin Institute of Technology, Harbin, 150001, China

ARTICLE INFO

Article history:
Received 17 January 2017
Revised 20 April 2017
Accepted 24 April 2017
Available online 27 April 2017

Keywords:
Direction-of-arrival (DOA) estimation
Real-valued computation
Arbitrary array configuration
Virtual array transformation

ABSTRACT

In this paper, we propose a reduced-complexity algorithm to estimate the direction of arrivals (DOAs) of multiple uncorrelated narrow-band signals. We show that with an array of arbitrary configuration, the real part of the array covariance matrix can be equivalently reformulated as an entire array covariance matrix received by a virtual array with potential signal model available for DOA estimate. We provide in-depth insights into the eigenvalue decomposition (EVD) on the real part of the array covariance matrix, based on which we propose a novel virtual array transformation multiple signal classification (VAT-MUSIC) algorithm for DOA estimation with efficient real-valued computations. The new algorithm is able to reduce about 75% computational complexity and it has easy implementation advantages over state-of-the-art real-valued techniques. Furthermore, the performance of the proposed algorithm is theoretically analyzed and a closed-form expression is derived to predict the mean square error (MSE) of the new DOA estimator. Numerical simulations are conducted to demonstrate the advantages of the proposed algorithm and to verify the theoretical analysis.

1. Introduction

Array signal processing for direction-of-arrival (DOA) estimation is one of the major interests in many applications including radar, sonar, and wireless communication [1–5]. Over several decades, this topic has been extensively studied and many algorithms, such as multiple signal classification (MUSIC) [6], minimum norm (MN) [7], estimation of the signal parameters via rotational invariance techniques (ESPRIT) [8], subspace fitting (SF) [9] and maximum likelihood (ML) [10], have been proposed. Among these existing DOA estimators, the MUSIC algorithm firstly exploits the orthogonality between the signal- and the noise- subspaces to achieve a super-resolution DOA estimation with efficient resolution for very closely-spaced sources. The most outstanding advantage of the MUSIC algorithm is its easy implementation with arbitrary array configurations. However, conventional MUSIC is computationally expensive since it involves a matrix decomposition step on the array covariance matrix and a tremendous spectral search step for final DOA estimates [11].

Noting that both tasks of matrix decomposition and spectral search involved in conventional MUSIC are implemented with complex-valued computations, a unitary transformation and a forward/backword (FB) averaging [12] techniques are proposed to reduce the complexity through real-valued arithmetics. These techniques are studied for the unitary MUSIC (U-MUSIC) algorithm [13] and extended to unitary root MUSIC (U-root-MUSIC) [14] [15], unitary ESPRIT (U-ESPRIT) [16], unitary method of direction-of-arrival estimation (U-MODE) [17] and unitary matrix pencil (U-MP) [18]. Based on the special structures of centro-symmetrical arrays (CSAs), those algorithms transform the complex array covariance matrix into a real one. It has been proven that this real matrix is symmetrical, and hence, both matrix decomposition and spectral search can be implemented with real-valued computations. Generally, one multiplication between two complex variables require four times that between two real ones, unitary algorithms hence reduce about 75% complexity as compared to their complex versions. Besides, it has been found that real-valued algorithms also show improved accuracy as compared to complex-valued approaches. Despite their increased estimation accuracies with reduced costs, almost all of the state-of-the-art real-valued methods are only suitable for CSAs, which severely limits their applications [19].

There have been promising techniques proposed under arbitrary array assumptions to exploit polynomial rooting for fast DOA estimation. These include array interpolation (AI) [20], beamspace

* Corresponding author.
E-mail address: dr.junshi@gmail.com (J. Shi).

http://dx.doi.org/10.1016/j.sigpro.2017.04.017
0165-1684/

transformation [21], manifold separation technique (MST) [22] and Fourier-domain (FD) root-MUSIC [23], which aim to map the steering vector of a nonuniform array (NUA) to that of a uniform linear array (ULA) with Vandermonde structure. Unfortunately, these algorithms generally sacrifice estimation accuracies due to mapping errors. It has been shown that AI introduces mapping errors which may cause increased bias and excess variance [24,25]. It has been also shown that polynomial rooting with a sufficiently high order is generally needed for MST and FD root-MUSIC to warrant sufficiently small truncation errors, which may cause higher additional complexities than expected [26].

In this paper, unlike the above mentioned methods that attempted to overcome the high complexity problem based on special array structures or with array mapping techniques, we show that exploiting only the real part of the array covariance matrix can lead to a real-valued version of the MUSIC algorithm for fast DOA estimate with no dependence on array configurations. We prove that the real part of the array covariance matrix can be equivalently reformulated as an entire array covariance matrix received by a virtual array with an extended array manifold which is real. Because the virtual array covariance matrix and the virtual array manifold are real, both tasks of matrix decomposition and spectral search can be implemented with efficient real-valued computations by a novel proposed virtual array transformation MUSIC (VAT-MUSIC) algorithm. The new algorithm is able to reduce about 75% computational complexity as compared to the standard MUSIC since it is a real-valued algorithm and it involves a limited spectral search over only half of the total angular-of-view. Furthermore, the developed technique also has implementation advantages over most state-of-the-art unitary techniques since it can be used with arbitrary arrays. We provide in-depth insights into the new approach including the eigenvalue decomposition (EVD) of the real-part of the array covariance matrix as well as the performance analysis. We derive a closed-form expression based on a high signal-to-noise SNR assumption to predict the mean square error (MSE) of the new DOA estimator.

Throughout the paper, vectors and matrices are denoted by lower- and upper- case boldface letters, respectively. In addition, Complex- and real-matrix are denoted by single-bar- and double-bar-upper boldface letters, respectively, and Re(·) and Im(·) denote the real- and the imaginary-parts of the embraced matrix, respectively.

2. Signal Model and Standard MUSIC

2.1. Signal Model

The problem of DOA estimation for L uncorrelated narrow-band plane waves impinging on an arbitrary linear array with M sensors located at $x_m, m = 1, 2, ..., M$ can be reduced to estimation of the unknown azimuthal angle parameter $\boldsymbol{\Theta} \triangleq \{\theta_1, \theta_2, \ldots, \theta_L\}$ in the equation

$$\mathbf{x}(t) = \mathbf{A}(\boldsymbol{\Theta})\mathbf{s}(t) + \mathbf{n}(t), \text{ for } t = 1, 2, \cdots, N \tag{1}$$

where

$\mathbf{x}(t) \in \mathbb{C}^{M\times 1}$	array output observed at snapshot t;
$\mathbf{A}(\boldsymbol{\Theta}) \in \mathbb{C}^{M\times L}$	array manifold matrix;
$\mathbf{s}(t) \in \mathbb{C}^{L\times 1}$	incident signal;
$\mathbf{n}(t) \in \mathbb{C}^{M\times 1}$	additive Gaussian white noise (AGWN).

The array manifold matrix is given by

$$\mathbf{A}(\boldsymbol{\Theta}) \triangleq [\mathbf{a}(\theta_1), \mathbf{a}(\theta_2), \ldots, \mathbf{a}(\theta_L)].$$

where each column

$$\mathbf{a}(\theta_l) \triangleq \left[e^{j\cdot 2\pi\cdot x_1\cdot \sin\theta_l/\lambda}, e^{j\cdot 2\pi\cdot x_2\cdot \sin\theta_l/\lambda}, \ldots, \quad e^{j\cdot 2\pi\cdot x_M\cdot \sin\theta_l/\lambda}\right]^T$$

is a so-called steering vector, where $j = \sqrt{-1}$ and λ is the center wavelength.

2.2. Basic Assumptions

The following basic assumptions on the data model (1) are considered to hold throughout the paper.

1) The number of sources is known [27] and is smaller than half that of sensors such that $L \leqslant \lfloor (M-1)/2 \rfloor$, where $\leq \lfloor \cdot \rfloor$ denotes rounding down to the nearest integer.
2) The positions and displacements of array elements do not need to be uniform or follow regular patterns, but they should satisfy the so-called rank-$(M-1)$ ambiguity restriction (see [28] and the references therein).
3) The AWGN $\mathbf{n}(t)$ satisfies

$$E\left[\mathbf{n}(t_i)\mathbf{n}^T(t_j)\right] = \mathbf{0} \tag{2a}$$

$$E\left[\mathbf{n}(t_i)\mathbf{n}^H(t_j)\right] = \delta(i-j)\sigma_n^2\mathbb{I}_M \tag{2b}$$

where $E[\cdot]$ is mathematical expectation, $(\cdot)^T$ and $(\cdot)^H$ are transpose and Hermitian transpose, respectively, σ_n^2 is noise power, $\mathbb{I}_M \in \mathbb{R}^{M\times M}$ is the $M \times M$ identity matrix, and $\delta(\cdot)$ is the Kronecker Delta function.
4) The incident signal $\mathbf{s}(t)$ is uncorrelated and satisfies

$$E\left[\mathbf{s}(t)\mathbf{s}^T(t)\right] = \mathbf{0} \tag{3a}$$

$$E\left[\mathbf{s}(t)\mathbf{s}^H(t)\right] = \mathbb{R}_s \tag{3b}$$

where $\mathbb{R}_s$ is the $M \times M$ real-valued diagonal source covariance (since $\mathbf{s}(t)$ is uncorrelated signal).

2.3. Standard MUSIC

Based on the above assumptions, we can compute the entire complex-valued array covariance matrix

$$\begin{aligned}\mathbf{R} &= E\left[\mathbf{x}(t)\mathbf{x}^H(t)\right] \\ &= \mathbf{A}(\boldsymbol{\Theta})E\left[\mathbf{s}(t)\mathbf{s}^H(t)\right]\mathbf{A}^H(\boldsymbol{\Theta}) + E\left[\mathbf{n}(t)\mathbf{n}^H(t)\right] \\ &= \mathbf{A}(\boldsymbol{\Theta})\mathbb{R}_s\mathbf{A}^H(\boldsymbol{\Theta}) + \sigma_n^2\mathbb{I}_M\end{aligned} \tag{4}$$

and write the EVD of $\mathbf{R}$ as follows

$$\mathbf{R} = \mathbf{U}_s\mathbf{Q}_s\mathbf{U}_s^H + \mathbf{U}_n\mathbf{Q}_n\mathbf{U}_n^H. \tag{5}$$

where $\mathbf{Q}_s \in \mathbb{C}^{L\times L}$ and $\mathbf{Q}_n \in \mathbb{C}^{(M-L)\times(M-L)}$ are two diagonal matrices, $\mathbf{U}_s \in \mathbb{C}^{M\times L}$ and $\mathbf{U}_n \in \mathbb{C}^{M\times(M-L)}$ are the so-called signal- and noise- matrices, which contain the eigenvectors relating to the L significant- and the $M-L$ smallest- eigenvalues of $\mathbf{R}$, respectively. In practical situations, the theoretical $\mathbf{R}$ in (4) is unavailable, and it is usually estimated by N snapshots of array received datum as follows

$$\widehat{\mathbf{R}} = \frac{1}{N}\sum_{t=1}^{N}\mathbf{x}(t)\mathbf{x}^H(t). \tag{6}$$

Therefore, the EVD of the array covariance matrix is in fact given by

$$\widehat{\mathbf{R}} = \widehat{\mathbf{U}}_s\widehat{\mathbf{\Pi}}_s\widehat{\mathbf{U}}_s^H + \widehat{\mathbf{U}}_n\widehat{\mathbf{\Pi}}_n\widehat{\mathbf{U}}_n^H. \tag{7}$$

According to the orthogonality between span($\mathbf{U}_s$) and span($\mathbf{U}_n$), the MUSIC algorithm [6] attempts to find the steering vectors which are as orthogonal to the estimated noise subspace as possible, in which source DOAs are found by an exhaustive point by point spectral search step as

$$p(\theta) = \left\|\mathbf{a}^H(\theta)\widehat{\mathbf{U}}_n\right\|^2. \tag{8}$$

Note that the standard MUSIC is computationally very expensive because for each point, the product $\left\|\mathbf{a}^H(\theta)\widehat{\mathbf{U}}_n\right\|^2$ must be computed [11].

3. The proposed VAT-MUSIC algorithm

3.1. Virtual Signal Model for the Real-Part of Array Covariance Matrix

In this subsection, we show that the real-part of the array covariance matrix contains a virtual signal model variable for DOA estimate. It follows directly from (4) that the the real-part of the array covariance matrix can be written as

$$\begin{aligned}\mathbb{R} &\triangleq \mathrm{Re}(\mathbf{R})\\ &= \mathrm{Re}\left[\mathbf{A}(\boldsymbol{\Theta})\mathbb{R}_s\mathbf{A}^H(\boldsymbol{\Theta})\right]+\sigma_n^2\mathbb{I}_M\\ &= \mathrm{Re}\left[\mathbf{B}(\boldsymbol{\Theta})\right]+\sigma_n^2\mathbb{I}_M\end{aligned} \tag{9}$$

where $\mathbf{B}(\boldsymbol{\Theta})\in\mathbb{C}^{M\times M}$ is defined as

$$\mathbf{B}(\boldsymbol{\Theta})\triangleq\mathbf{A}(\boldsymbol{\Theta})\mathbb{R}_s\mathbf{A}^H(\boldsymbol{\Theta}).$$

Using $\mathbf{A}(\boldsymbol{\Theta})=\mathrm{Re}[\mathbf{A}(\boldsymbol{\Theta})]+j\mathrm{Im}[\mathbf{A}(\boldsymbol{\Theta})]$, we have

$$\begin{aligned}\mathbf{B}(\boldsymbol{\Theta}) &= \left\{\mathrm{Re}[\mathbf{A}(\boldsymbol{\Theta})]+j\mathrm{Im}[\mathbf{A}(\boldsymbol{\Theta})]\right\}\cdot\mathbb{R}_s\\ &\quad\cdot\left\{\mathrm{Re}^T\left[\mathbf{A}(\boldsymbol{\Theta})\right]-j\mathrm{Im}^T\left[\mathbf{A}(\boldsymbol{\Theta})\right]\right\}\\ &= \mathrm{Re}\left[\mathbf{A}(\boldsymbol{\Theta})\right]\mathbb{R}_s\mathrm{Re}^T\left[\mathbf{A}(\boldsymbol{\Theta})\right]\\ &\quad+\mathrm{Im}\left[\mathbf{A}(\boldsymbol{\Theta})\right]\mathbb{R}_s\mathrm{Im}^T\left[\mathbf{A}(\boldsymbol{\Theta})\right]\\ &\quad+j\cdot\mathrm{Im}\left[\mathbf{A}(\boldsymbol{\Theta})\right]\mathbb{R}_s\mathrm{Re}^T\left[\mathbf{A}(\boldsymbol{\Theta})\right]\\ &\quad-j\cdot\mathrm{Re}\left[\mathbf{A}(\boldsymbol{\Theta})\right]\mathbb{R}_s\mathrm{Im}^T\left[\mathbf{A}(\boldsymbol{\Theta})\right].\end{aligned} \tag{10}$$

Therefore, $\mathrm{Re}\left[\mathbf{B}(\boldsymbol{\Theta})\right]$ can be written as

$$\begin{aligned}\mathrm{Re}\left[\mathbf{B}(\boldsymbol{\Theta})\right] &= \mathrm{Re}\left[\mathbf{A}(\boldsymbol{\Theta})\right]\mathbb{R}_s\mathrm{Re}^T\left[\mathbf{A}(\boldsymbol{\Theta})\right]\\ &\quad+\mathrm{Im}\left[\mathbf{A}(\boldsymbol{\Theta})\right]\mathbb{R}_s\mathrm{Im}^T\left[\mathbf{A}(\boldsymbol{\Theta})\right]\\ &= \left[\mathrm{Re}\left[\mathbf{A}(\boldsymbol{\Theta})\right]\ \mathrm{Im}\left[\mathbf{A}(\boldsymbol{\Theta})\right]\right]\times\begin{bmatrix}\mathbb{R}_s & \mathbf{0}\\ \mathbf{0} & \mathbb{R}_s\end{bmatrix}\\ &\quad\times\begin{bmatrix}\mathrm{Re}^T\left[\mathbf{A}(\boldsymbol{\Theta})\right]\\ \mathrm{Im}^T\left[\mathbf{A}(\boldsymbol{\Theta})\right]\end{bmatrix}\\ &\triangleq \mathbb{A}_{\mathrm{virtual}}(\boldsymbol{\Theta})\mathbb{R}_s^{\mathrm{virtual}}\mathbb{A}_{\mathrm{virtual}}^T(\boldsymbol{\Theta}).\end{aligned} \tag{11}$$

where $\mathbb{R}_s^{\mathrm{virtual}}\in\mathbb{R}^{2L\times 2L}$ and $\mathbb{A}_{\mathrm{virtual}}(\boldsymbol{\Theta})\in\mathbb{R}^{M\times 2L}$ are given by

$$\mathbb{R}_s^{\mathrm{virtual}}\triangleq\begin{bmatrix}\mathbb{R}_s & \mathbf{0}\\ \mathbf{0} & \mathbb{R}_s\end{bmatrix}$$

$$\mathbb{A}_{\mathrm{virtual}}(\boldsymbol{\Theta})\triangleq\left[\mathrm{Re}\left[\mathbf{A}(\boldsymbol{\Theta})\right]\ \mathrm{Im}\left[\mathbf{A}(\boldsymbol{\Theta})\right]\right].$$

Using (3), $\mathbb{R}_s^{\mathrm{virtual}}$ can be written as

$$\begin{aligned}\mathbb{R}_s^{\mathrm{virtual}} &= \begin{bmatrix}E\left[\mathbf{s}(t)\mathbf{s}^H(t)\right] & E\left[\mathbf{s}(t)\mathbf{s}^T(t)\right]\\ E\left[\mathbf{s}^*(t)\mathbf{s}^H(t)\right] & E\left[\mathbf{s}^*(t)\mathbf{s}^T(t)\right]\end{bmatrix}\\ &\triangleq E\left[\mathbf{s}_{\mathrm{virtual}}(t)\mathbf{s}_{\mathrm{virtual}}^H(t)\right]\end{aligned} \tag{12}$$

where $\mathbf{s}_{\mathrm{virtual}}(t)\in\mathbb{C}^{2L\times 1}$ is given by

$$\mathbf{s}_{\mathrm{virtual}}(t)\triangleq\begin{bmatrix}\mathbf{s}(t)\\ \mathbf{s}^*(t)\end{bmatrix}.$$

Inserting (11) into (9) and using (12) leads to

$$\begin{aligned}\mathbb{R} &= \mathbb{A}_{\mathrm{virtual}}(\boldsymbol{\Theta})\mathbb{R}_s^{\mathrm{virtual}}\mathbb{A}_{\mathrm{virtual}}^T(\boldsymbol{\Theta})+\sigma_n^2\mathbb{I}_M\\ &= \mathbb{A}_{\mathrm{virtual}}(\boldsymbol{\Theta})E\left[\mathbf{s}_{\mathrm{virtual}}(t)\mathbf{s}_{\mathrm{virtual}}^H(t)\right]^H\mathbb{A}_{\mathrm{virtual}}^H(\boldsymbol{\Theta})\\ &\quad+\sigma_n^2\mathbb{I}_M\\ &= E\left\{\left[\mathbb{A}_{\mathrm{virtual}}(\boldsymbol{\Theta})\mathbf{s}_{\mathrm{virtual}}(t)+\mathbf{n}(t)\right]\right.\\ &\quad\left.\times\left[\mathbb{A}_{\mathrm{virtual}}(\boldsymbol{\Theta})\mathbf{s}_{\mathrm{virtual}}(t)+\mathbf{n}(t)\right]^H\right\}\\ &\triangleq E\left[\mathbf{x}_{\mathrm{virtual}}(t)\mathbf{x}_{\mathrm{virtual}}^H(t)\right]\end{aligned} \tag{13}$$

where $\mathbf{x}_{\mathrm{virtual}}(t)\in\mathbb{C}^{M\times 1}$ is given by

$$\mathbf{x}_{\mathrm{virtual}}(t)\triangleq\mathbb{A}_{\mathrm{virtual}}(\boldsymbol{\Theta})\mathbf{s}_{\mathrm{virtual}}(t)+\mathbf{n}(t).$$

Comparing (13) with (4), the real-part of the array covariance matrix can be regarded as an entire array covariance matrix of a virtual array with a manifold matrix $\mathbb{A}_{\mathrm{virtual}}(\boldsymbol{\Theta})$. The output sensor vector of this virtual array is $\mathbf{x}_{\mathrm{virtual}}(t)$ and the incident signal on this virtual array is $\mathbf{s}_{\mathrm{virtual}}(t)$ with its covariance matrix given by $\mathbb{R}_s^{\mathrm{virtual}}$.

3.2. The proposed VAT-MUSIC method

Since DOA information is also contained in $\mathbb{A}_{\mathrm{virtual}}(\boldsymbol{\Theta})$, we now exploit the idea of eigenvalue analysis to perform the EVD of the virtual array covariance matrix $\mathbb{R}$ and construct a MUSIC-like spectral for DOA estimate.

Because $\mathbb{R}=\mathbb{R}^T$, the EVD of $\mathbb{R}$

$$\mathbb{R}=\mathbb{U}\mathbb{Q}\mathbb{U}^T \tag{14}$$

requires only real-valued computations [29]. Using (4), we show in Appendix A that the eigenvalues of $\mathbb{R}$ are given by

$$\xi_i=\begin{cases}\alpha_i+\sigma_n^2, & i=1,2,\ldots,2L-K\\ \sigma_n^2, & i=2L-K+1,2,\ldots,M\end{cases} \tag{15}$$

where $\alpha_1,\alpha_2,\ldots,\alpha_{2L-K}$ are the $2L-K$ eigenvalues of $\mathbb{B}(\boldsymbol{\Theta})\mathbb{R}_s^{\mathrm{virtual}}\mathbb{B}^T(\boldsymbol{\Theta})$, $K(K\le\lfloor L/2\rfloor)$ is number of pairs of symmetrical sources in $\boldsymbol{\Theta}$ and $\mathbb{B}(\boldsymbol{\Theta})$ is defined as

$$\mathbb{B}(\boldsymbol{\Theta})\triangleq\frac{1}{\sqrt{2}}\left[\mathbf{A}(\boldsymbol{\Theta})\ \mathbf{A}^*(\boldsymbol{\Theta})\right].$$

Therefore, $\mathbb{R}$ has $2L-K$ significant- and $M-2L+K$ smallest-eigenvalues, and the EVD of $\mathbb{R}$ can be rewritten as

$$\begin{aligned}\mathbb{R} &= \sum_{i=1}^{2L-K}\xi_i\mathbb{u}_i\mathbb{u}_i^H+\sum_{j=2L-K+1}^{M}\xi_j\mathbb{u}_j\mathbb{u}_j^H\\ &= \mathbb{U}_s\mathbb{Q}_s\mathbb{U}_s^H+\mathbb{U}_n\mathbb{Q}_n\mathbb{U}_n^H\end{aligned} \tag{16}$$

where the signal matrix $\mathbb{U}_s\in\mathbb{R}^{M\times(2L-K)}$ and the noise matrix $\mathbb{U}_n\in\mathbb{R}^{M\times(M-2L+K)}$ contain eigenvectors associated with the $2L-K$ significant- and the $M-2L+K$ smallest- eigenvalues of $\mathbb{R}$, respectively.

$$\mathbb{Q}_s\triangleq\mathrm{diag}\left\{\xi_1,\xi_2,\ldots,\xi_{2L-K}\right\} \tag{17a}$$

$$\mathbb{Q}_n\triangleq\mathrm{diag}\left\{\xi_{2L-K+1},\xi_{2L-K+2},\ldots,\xi_M\right\} \tag{17b}$$

$$\mathbb{U}_s\triangleq\left[\mathbb{u}_1,\mathbb{u}_2,\ldots,\mathbb{u}_{2L-K}\right] \tag{17c}$$

$$\mathbb{U}_n\triangleq\left[\mathbb{u}_{2L-K+1},\mathbb{u}_{2L-K+2},\ldots,\mathbb{u}_M\right]. \tag{17d}$$

According to (13), $\mathbb{A}_{\mathrm{virtual}}(\boldsymbol{\Theta})$ is the virtual manifold matrix associated with $\mathbb{R}$. Therefore, by using the orthogonality between the signal- and the noise- subspaces, we obtain

$$\mathrm{span}\left(\mathbb{U}_s\right)\perp\mathrm{span}\left(\mathbb{U}_n\right) \tag{18a}$$

Table 1
The proposed VAT-MUSIC algorithm.

- **Step 1**: Estimate $\widehat{\mathbf{R}}$ by (6) and obtain $\widehat{\mathbb{R}}$.
- **Step 2**: Perform EVD on $\widehat{\mathbb{R}}$ by (16) to obtain $\widehat{\mathbb{U}}_n$;
- **Step 3**: Construct $f(\theta)$ by (20);
- **Step 4**: Search $f(\theta)$ over $[0, \pi/2]$ (or $[-\pi/2, 0]$) to obtain $\widehat{\boldsymbol{\theta}} \triangleq \{\widehat{\theta}_1, \widehat{\theta}_2, ..., \widehat{\theta}_T\}$, $T < L$;
- **Step 5**: Select the L true DOAs among the $2T$ candidate angels $\{\widehat{\boldsymbol{\theta}}, -\widehat{\boldsymbol{\theta}}\}$ by maximizing $\|\mathbf{a}^H(\theta)\widehat{\mathbf{R}}\mathbf{a}(\theta)\|^2$.

$$\text{span}\left(\mathbb{U}_s\right) = \text{span}\left[\mathbb{A}_{\text{virtual}}(\boldsymbol{\Theta})\right]. \tag{18b}$$

Because $\mathbb{A}_{\text{virtual}}(\boldsymbol{\Theta}) = [\text{Re}[\mathbf{A}(\Theta)]\ \text{Im}[\mathbf{A}(\Theta)]]$ is in fact a combined manifold matrix covering both $\text{Re}[\mathbf{A}(\Theta)]$ and $\text{Im}[\mathbf{A}(\Theta)]$, we have

$$\text{span}[\mathbb{A}_{\text{virtual}}(\boldsymbol{\Theta})] = \text{span}\Big\{\mathbb{a}_{\text{re}}(\theta_1), \mathbb{a}_{\text{re}}(\theta_2), \cdots, \mathbb{a}_{\text{re}}(\theta_L), \mathbb{a}_{\text{im}}(\theta_1), \mathbb{a}_{\text{im}}(\theta_2), \cdots, \mathbb{a}_{\text{im}}(\theta_L)\Big\} \tag{19}$$

where $\mathbb{a}_{\text{re}}(\theta) \triangleq \text{Re}\left[\mathbf{a}(\theta)\right] \in \mathbb{R}^{M\times 1}$ and $\mathbb{a}_{\text{im}}(\theta) \triangleq \text{Im}\left[\mathbf{a}(\theta)\right] \in \mathbb{R}^{M\times 1}$ are two real vectors, given by

$$\begin{aligned}\mathbb{a}_{\text{re}}(\theta) &\triangleq \text{Re}[\mathbf{a}(\theta)] \\ &= \left[\cos\left(\frac{2\pi}{\lambda}\cdot x_1\cdot\sin\theta\right), \cos\left(\frac{2\pi}{\lambda}\cdot x_2\cdot\sin\theta\right), \cdots, \cos\left(\frac{2\pi}{\lambda}\cdot x_M\cdot\sin\theta\right)\right]^T\end{aligned}$$

$$\begin{aligned}\mathbb{a}_{\text{im}}(\theta) &\triangleq \text{Im}[\mathbf{a}(\theta)] \\ &= \left[\sin\left(\frac{2\pi}{\lambda}\cdot x_1\cdot\sin\theta\right), \sin\left(\frac{2\pi}{\lambda}\cdot x_2\cdot\sin\theta\right), \cdots, \sin\left(\frac{2\pi}{\lambda}\cdot x_M\cdot\sin\theta\right)\right]^T.\end{aligned}$$

Based on (A.3) and (19), we can define a MUSIC-like spectral for DOA estimation as follows

$$f(\theta) = \left\|\mathbb{a}_{\text{re}}^T(\theta)\widehat{\mathbb{U}}_n\right\|^2 + \left\|\mathbb{a}_{\text{im}}^T(\theta)\widehat{\mathbb{U}}_n\right\|^2. \tag{20}$$

Since $\mathbb{a}(\theta) = \mathbb{a}(-\theta)$ and $\mathbb{b}(\theta) = \mathbb{b}(-\theta)$, mirror peaks are caused by VAT-MUSIC. Therefore, if $\widehat{\theta}$ is a DOA, VAT-MUSIC must show two peaks at $\widehat{\theta}$ and $-\widehat{\theta}$ simultaneously. To solve the problem of ambiguity, the conventional beamformer (CBF) [30] is applied here to select the true DOA between $\widehat{\theta}$ and $-\widehat{\theta}$ by maximizing $\|\mathbf{a}^H(\theta)\widehat{\mathbf{R}}\mathbf{a}(\theta)\|$.

Since $\mathbb{U}_n$ is of dimensions $M \times (M - 2L + K)$, one should know both L and K to obtain $\mathbb{U}_n$ from the EVD of $\mathbb{R}$. However, this requires an addition assumption for the knowledge of K, which is difficult to determine in practice. Considering that it may be rare that two sources are exactly the mirrored versions of each other, we can select the $M - 2L$ (instead of $M - 2L + K$) smallest vectors of $\mathbb{R}$ to obtain matrix $\mathbb{U}_n$. This means we reduce the dimension of $\mathbb{U}_n$, and use its $M - 2L$ columns to construct the VAT-MUSIC spectral. Although the dimension reduction may sacrifice a slight accuracy, it is to be shown by both theoretical analysis and simulations that the proposed method performs closely to the standard MUSIC.

3.3. Summary and Complexity Analysis

Detailed steps for implementing the proposed VAT-MUSIC algorithm for real-valued DOA estimation with arbitrary array configurations are summarized in Table 1.

Table 2 compares the primary real-valued complexity between standard MUSIC and the proposed VAT-MUSIC algorithm. Because the EVD and spectral search step dominate the total complexity, the common flops required for the computation of $\widehat{\mathbf{R}}$ by the two methods and those required by VAT-MUSIC for solving the ambiguity problem can be omitted. Using the fast subspace decomposition (FSD) technique [31], the EVD of $\widehat{\mathbb{R}}$ costs $M^2(2L - K + 2)$ flops. Since $\widehat{\mathbf{R}}$ is complex, its EVD requires $4 \times M^2(L + 2)$ flops. For J sample points over $[-\pi/2, \pi/2]$, VAT-MUSIC only need to compute $J/2$ spectral points. As $\mathbb{a}_{\text{re}}(\theta) \in \mathbb{R}^{M\times 1}$, $\mathbb{a}_{\text{im}}(\theta) \in \mathbb{R}^{M\times 1}$ and $\mathbb{U}_n \in \mathbb{R}^{M\times(M-2L+K)}$, the spectral search for VAT-MUSIC costs $J(M + 1)(M - 2L + K)$ flops [11,29]. Because $\mathbf{a}(\theta) \in \mathbb{C}^{M\times 1}$, $\mathbf{U}_n \in \mathbb{C}^{M\times(M-L)}$ and J points must be computed, the standard MUSIC costs $4 \times J(M + 1)(M - L)$ flops for the spectral search step. Generally, we have $J \gg M$ [11], therefore, the proposed method reduces about 75% flops as compared to the standard MUSIC.

Table 2
Comparison of real-valued computational complexity.

Algorithms	Primary real-valued computations
MUSIC	$4 \times \left[M^2(L + 2) + J(M + 1)(M - L)\right]$
VAT-MUSIC	$M^2(2L - K + 2) + J(M + 1)(M - 2L + K)$

4. Performance Analysis

In this section, we derive a closed-from expression to theoretically predict the MSE of DOA estimation by VAT-MUSIC base on a high (SNR) assumption. To this end, we introduce a direct-data (noise-free) matrix

$$\mathbf{X} \triangleq \mathbf{A}(\boldsymbol{\Theta})[\mathbf{s}(1), \mathbf{s}(2), \ldots, \mathbf{s}(N)]$$

as well as the following two lemmas [32,33]

Lemma 1. *Assume the SVD of* $\mathbf{X}$ *is given by*

$$\mathbf{X} = \mathbf{X}_s\boldsymbol{\Pi}_s\mathbf{Y}_s^H + \mathbf{X}_n\boldsymbol{\Pi}_n\mathbf{Y}_n^H \tag{21}$$

the perturbation of the noise matrix $\mathbf{U}_n$ *equals to the perturbation of* $\mathbf{X}_n$*, and it can be expressed by a linear function of* $\mathbf{N}$ *at high* SNR*s as*

$$\Delta\mathbf{U}_n = \Delta\mathbf{X}_n = -\mathbf{X}_s\boldsymbol{\Pi}_s^{-1}\mathbf{Y}_s^H\mathbf{N}^H\mathbf{X}_n. \tag{22}$$

Lemma 2. *Assume the AGWNs are Gaussian random variables with zero means and variance* σ_n^2 *and let* $\mathbf{d}(\theta_l) \triangleq d\mathbf{a}(\theta_l)/d\theta_l$ *denote the first-order derivation of* $\mathbf{a}(\theta_l)$ *respect to* θ_l*, the MSE for DOA estimation by the standard MUSIC at high* SNR *is given by*

$$\text{MSE}_{\text{MUSIC}}\left(\widehat{\theta}_l\right) = \frac{\sigma_n^2\|\alpha_l\|^2}{2|\gamma_l|} \tag{23}$$

where $\boldsymbol{\alpha}_l$*,* $\boldsymbol{\gamma}_l$ *are defined as follows*

$$\alpha_l \triangleq \mathbf{Y}_s\boldsymbol{\Pi}_s^{-1}\mathbf{X}_s^H\mathbf{a}(\theta_l)$$

$$\gamma_l \triangleq \mathbf{d}^H(\theta_l)\mathbf{U}_n\mathbf{U}_n^H\mathbf{d}(\theta_l).$$

Now, we use the original noise-free matrix $\mathbf{X}$ *to define a virtual direct-data matrix*

$$\mathbf{X}_{\text{virtual}} \triangleq [\mathbf{X} \quad \mathbf{X}^*]$$

and write its SVD as follows

$$\mathbf{X}_{\text{virtual}} = \mathbf{E}_s\mathbf{W}_s\mathbf{F}_s^H + \mathbf{E}_n\mathbf{W}_n\mathbf{F}_n^H. \tag{24}$$

Using lemma 1, we show in Appendix B that the perturbation of the noise matrix $\mathbb{U}_n$ *can be expressed by a linear function of matrix* $\widetilde{\mathbf{N}}$ *as*

$$\Delta\mathbb{U}_n = -\mathbf{E}_s\mathbf{W}_s^{-1}\mathbf{F}_s^H\widetilde{\mathbf{N}}^H\mathbb{U}_n \tag{25}$$

where

$$\widetilde{\mathbf{N}} \triangleq [\mathbf{N} \quad \mathbf{N}^*], \quad \mathbf{N} \triangleq [\mathbf{n}(1), \mathbf{n}(2), \ldots, \mathbf{n}(N)].$$

Using (25), we show in Appendix C that the MSE for DOA estimation by the proposed VAT-MUSIC at high SNR *is given by*

$$\text{MSE}_{\text{VAT-MUSIC}}\left(\widehat{\theta}_l\right) = \sigma_n^2\frac{\|\boldsymbol{p}_1\|^2\|\mathbb{q}_1\|^2 + \|\boldsymbol{p}_2\|^2\|\mathbb{q}_2\|^2}{|m_1 + m_2|^2} \tag{26}$$

Table 3
MRLA configurations.

number of sensors	sequence
10	0, 1, 5, 9, 16, 23, 30, 33, 35, 36
12	0, 1, 5, 9, 16, 23, 30, 37, 44, 47, 49, 50
13	0, 1, 5, 8, 12, 21, 30, 39, 48, 53, 54, 56, 58
14	0, 1, 2, 8, 14, 20, 31, 42, 53, 58, 63, 66, 67, 68

where

$$\mathbf{p}_1 \triangleq \mathbf{F}_s\mathbf{W}_s^{-1}\mathbf{E}_s^H\mathbb{a}_{\mathrm{re}}(\theta_l)$$
$$\mathbb{q}_1 \triangleq \mathbb{U}_n\mathbb{U}_n^T\mathbb{d}_{\mathrm{re}}(\theta_l)$$
$$m_1 \triangleq \mathbb{d}_{\mathrm{re}}^T(\theta_l)\mathbb{U}_n\mathbb{U}_n^T\mathbb{d}_{\mathrm{re}}(\theta_l)$$
$$\mathbf{p}_2 \triangleq \mathbf{F}_s\mathbf{W}_s^{-1}\mathbf{E}_s^H\mathbb{a}_{\mathrm{im}}(\theta_l)$$
$$\mathbb{q}_2 \triangleq \mathbb{U}_n\mathbb{U}_n^T\mathbb{d}_{\mathrm{im}}(\theta_l)$$
$$m_2 \triangleq \mathbb{d}_{\mathrm{im}}^T(\theta_l)\mathbb{U}_n\mathbb{U}_n^T\mathbb{d}_{\mathrm{im}}(\theta_l)$$

with $\mathbb{d}_{\mathrm{re}}(\theta_l) \triangleq d\mathbb{a}_{\mathrm{re}}(\theta_l)/d\theta_l$ *and* $\mathbb{d}_{\mathrm{im}}(\theta_l) \triangleq d\mathbb{a}_{\mathrm{im}}(\theta_l)/d\theta_l$ *denoting the first-order derivations of* $\mathbb{a}_{\mathrm{re}}(\theta_l)$ *and* $\mathbb{a}_{\mathrm{im}}(\theta_l)$ *respect to* θ_l*, respectively.*

5. Simulation results

Numerical simulations are conducted to assess the performance of the proposed method and to verify the theoretical performance analysis. Throughout the simulations, 1000 independent Monte-Carlo trials have been used on a minimum redundancy linear array (MRLA) whose configuration is given in Table 3 [34]. Note that the centro-symmetrical structure does not exist in a MRLA, and hence most state-of-the-art real-valued methods [13]~ [18] cannot be used in such an array directly without array mapping technique [35].

For the root MSE (RMSE) comparison, the unconditional Cramer–Rao lower bound (CRLB) [36] is applied for a common reference, where the RMSE for the estimates of source incident angle θ is defined as

$$\mathrm{RMSE} \triangleq \sqrt{\frac{1}{1000}\sum_{i=1}^{1000}(\widehat{\theta}_i - \theta)^2}$$

where θ is the true DOA and $\widehat{\theta}_i$ represents the estimated value of the DOA of the ith trial. For L sources, the SNR is defined as

$$\mathrm{SNR} \triangleq 10\log_{10}\left[\frac{P_{\mathrm{avg}}}{\sigma_n^2}\right]$$

where $P_{\mathrm{avg}} = \frac{1}{L}\sum_{l=1}^{L}P_l$ denotes the average power of all sources, and $P_l = E\left[\mathbf{s}_l^2(t)\right]$ is the power of the lth, $l \in [1, L]$ source.

In the first simulation, we compare the spectrums of different algorithms including CBF, MUSIC and the proposed VAT-MUSIC. In the simulation, a MRLA with $M = 14$ sensors is used to estimate $L = 3$ sources at $\theta_1 = -20^\circ - \delta$, $\theta_2 = 20^\circ$ and $\theta_3 = 40^\circ$. We set $\delta = 0^\circ$ and $\delta = 0.3^\circ$ and plot spectrums of the three methods in Figs. 1 and 2, respectively.

It is seen from Fig. 1 that with $\delta = 0^\circ$, we have $\theta_1 = -\theta_2$, and there are $K = 1$ pair of symmetrical peaks in the spectral of VAT-MUSIC. As the mirror peak of θ_1 overlaps that of θ_2, and vice versa, there are only 4 peaks at -40°, -20°, 20°, 40°. However, this does not effect the correctness of the proposed method because by performing Step 5 in Table 1, $L = 3$ angles -20°, 20°, 40° are selected from the four candidate angles as the true DOAs since the CBF takes $L = 3$ maximal values A_1, A_2, A_3 at those directions.

On the other hand, with $\delta = 0.3^\circ$, we have $\theta_1 \approx -\theta_2$ but $\theta_1 \neq -\theta_2$. Theoretically, since $\theta_1 \neq -\theta_2$, there should be 6 candidate angles -40°, -20.3°, -20°, 20°, 20.3°, 40° for VAT-MUSIC. However, as the mirror of θ_1 lies too close to θ_2 and vice versa, there are only 4 peaks for VAT-MUSIC at -40°, -20.19°, 20.24°, 40°, as shown clearly in Fig. 2. Nevertheless, by performing Step 5 in Table 1, $L = 3$ angles -20.19°, 20.24°, 40° are selected from the four candidate angles -40°, -20.19°, 20.24°, 40° as true DOAs since the CBF takes $L = 3$ maximal values A_1, A_2, A_3 at those directions. Considering the estimation accuracy of VAT-MUSIC may deteriorate slightly in such a case, we suggest to use the standard MUSIC around the estimated angles by VAT-MUSIC to enhance estimation accuracy.

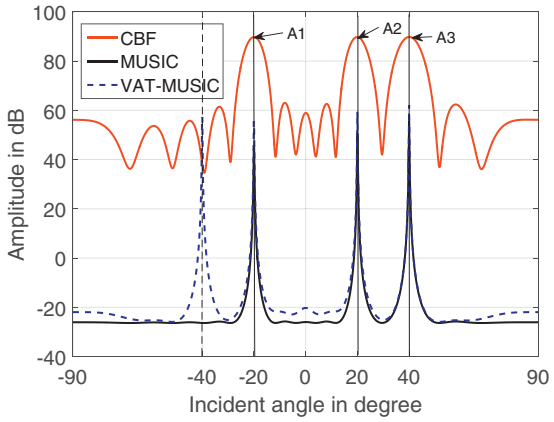

Fig. 1. Spectral with two symmetrical sources. MRLA, $M = 14$, $L = 3$, SNR = 10dB, $N = 100$, $\theta_1 = -20^\circ$, $\theta_2 = 20^\circ$, $\theta_3 = 40^\circ$.

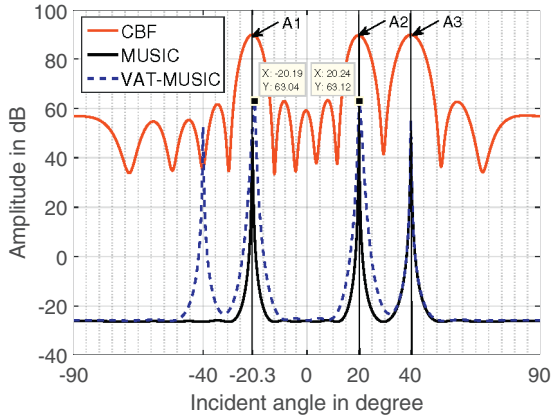

Fig. 2. Spectral with two approximately symmetrical sources. MRLA, $M = 14$, $L = 3$, SNR = 10dB, $N = 100$, $\theta_1 = -20.3^\circ$, $\theta_2 = 20^\circ$, $\theta_3 = 40^\circ$.

In the second simulation, we examine the RMSE performance of the proposed method and compare it to that of the standard MUSIC. In the simulation, a MRLA with $M = 12$ sensors is used to estimate $L = 2$ sources at $\theta_1 = 30^\circ$ and $\theta_2 = 40^\circ$. For both the two methods, a coarse gird 1.1° is firstly used to get candidate peaks, and a fine one 0.0051° is secondly applied around the candidate peaks for final DOA estimates.

Fig. 3 plots the RMSEs as functions of the SNR, where the number of snapshots is set as $N = 100$ and the SNR varies over a wide range from SNR = 0dB to SNR = 40dB. It can be concluded from Fig. 3 that with a significantly reduced computational complexity, the proposed method is still able to provide a very close RMSE to the standard MUSIC.

To see more clearly the performance of the new approach, Fig. 4 plots RMSEs of both the two algorithms as functions of the number of snapshots, where the SNR is set as SNR = 5dB and the number of snapshots varies from $N = 50$ to $N = 450$. It can be observed

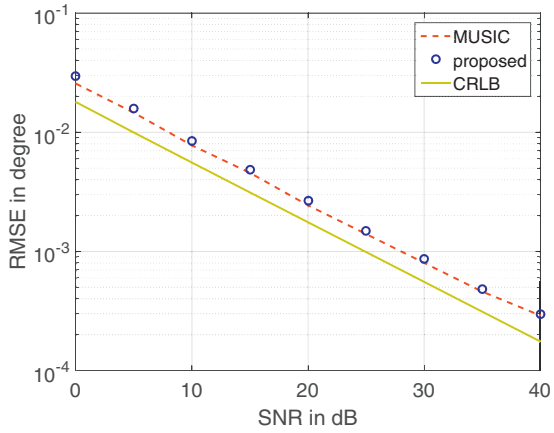

Fig. 3. RMSEs against the SNR respect to $\theta_1 = 30^\circ$, MRLA, $M = 12$ sensors, $N = 100$ snapshots, $L = 2$ sources at $\theta_1 = 30^\circ$ and $\theta_2 = 40^\circ$.

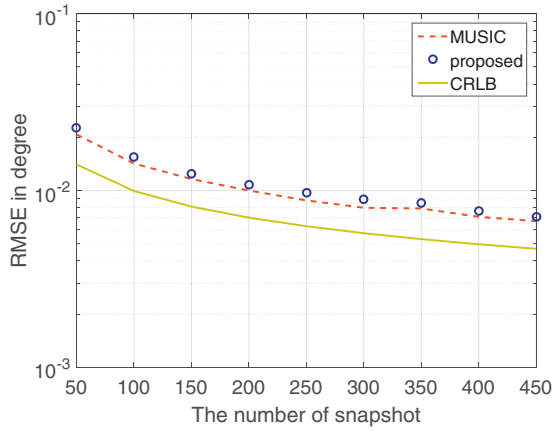

Fig. 4. RMSEs against the number of snapshot respect to $\theta_1 = 30^\circ$, MRLA, $M = 12$ sensors, SNR = 5dB, $L = 2$ sources at $\theta_1 = 30^\circ$ and $\theta_2 = 40^\circ$.

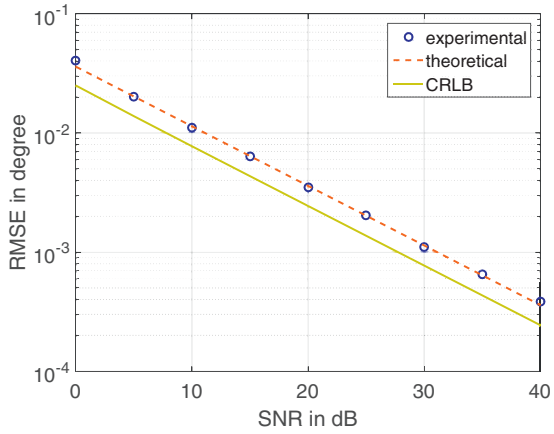

Fig. 5. Experimental- and theoretical- RMSEs against the SNR respect to $\theta_1 = 20^\circ$, MRLA, $M = 10$ sensors, $N = 100$ snapshots, $L = 2$ sources at $\theta_1 = 20^\circ$ and $\theta_2 = 30^\circ$.

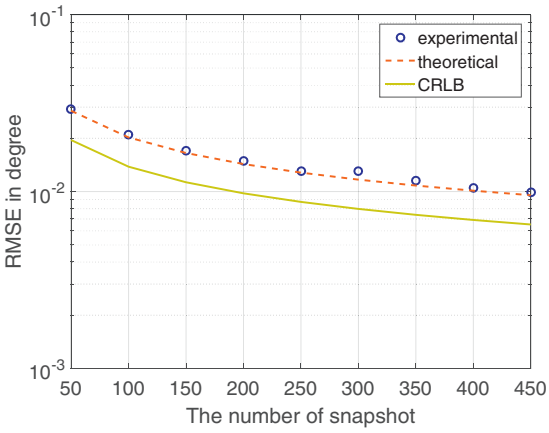

Fig. 6. Experimental- and theoretical- RMSEs against the number of snapshot respect to $\theta_1 = 20^\circ$, MRLA, $M = 10$ sensors, SNR = 5dB, $L = 2$ sources at $\theta_1 = 20^\circ$ and $\theta_2 = 30^\circ$.

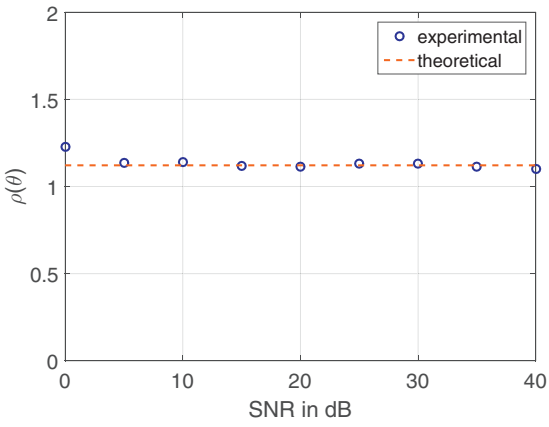

Fig. 7. RMSE relative efficiency between MUSIC and VAT-MUSIC against the SNR respect to $\theta_1 = 20^\circ$, MRLA, $M = 10$ sensors, $N = 100$ snapshots, $L = 2$ sources at $\theta_1 = 20^\circ$ and $\theta_2 = 30^\circ$.

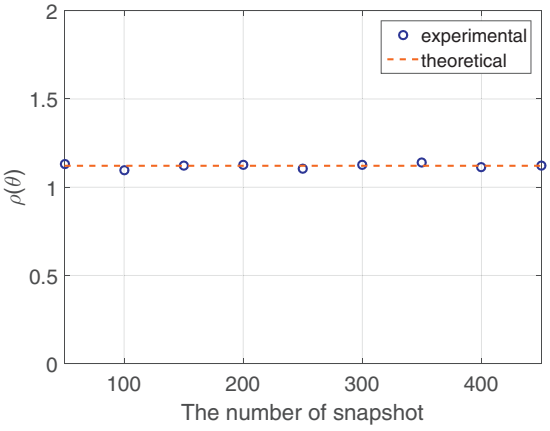

Fig. 8. RMSE relative efficiency between MUSIC and VAT-MUSIC against the number of snapshot respect to $\theta_1 = 20^\circ$, MRLA, $M = 10$ sensors, SNR = 5dB, $L = 2$ sources at $\theta_1 = 20^\circ$ and $\theta_2 = 30^\circ$.

again from Fig. 4 that the proposed technique performs similarly to the standard MUSIC. Therefore, the proposed algorithm provides an efficient performance-to-complexity tradeoff as compared to the standard MUSIC.

In the second simulation, we verify the theoretical MSE expression for DOA estimates by the proposed algorithm with a MRLA of $M = 10$ sensors. In Figs. 5 and 6, we compare the simulated RMSEs with those computed by (26) with the SNR and the number of snapshot, respectively. In Figs. 7 and 8 we compare the RMSE gap between MUSIC and VAT-MUSIC against the SNR and the number of snapshot, respectively, where the RMSE gap is defined as the relative efficiency between the two estimators

$$\rho\left(\widehat{\theta}_l\right) \triangleq \frac{\mathrm{MSE}_{\mathrm{VAT-MUSIC}}\left(\widehat{\theta}_l\right)}{\mathrm{MSE}_{\mathrm{MUSIC}}\left(\widehat{\theta}_l\right)}$$

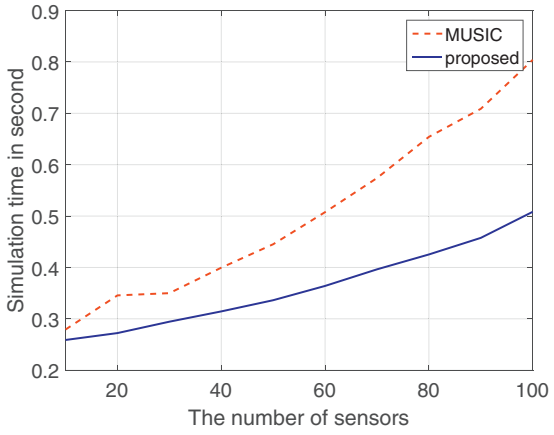

Fig. 9. Simulation time against the number of sensors, MRLA, SNR = 5dB, $N = 100$ snapshots, $L = 2$ sources at $\theta_1 = 30^\circ$ and $\theta_2 = 40^\circ$.

We compare simulated values with theoretical ones computed by using (23) and (26) for MUSIC and VAT-MUSIC, respectively.

It is seen clearly from Figs. 5 and 6 that there is a close match between the simulated RMSEs for DOA estimation by VAT-MUSIC and their theoretical expectations. It is also seen from Figs. 7 and 8 the simulated RMSE relative efficiency between MUSIC and the proposed method match their theoretical predictions. These observations verify the theoretical analysis in Section 4. Furthermore, the RMSE relative efficiency between the two methods are small (smaller than 1.2 as shown in Figs. 7 and 8), which implies that VAT-MUSIC reduces the complexity and keeps estimation accuracy comparable with the standard MUSIC.

In the last simulation, we verify the efficiency of the proposed approach by comparing the simulation times of DOA estimates by MUSIC and VAT-MUSIC as functions of the number of sensors in Fig. 9. The simulated results are given by a PC with Intel(R) Core(TM) Duo T5870 2.0 GHz CPU and 1GB RAM by running the Matlab codes in the same environment. It can be seen from Fig. 9 that the proposed method costs a much lower simulation time than the standard MUSIC, especially for large numbers of sensors. Note that the proposed method and MUSIC include a common step for the computation of $\widehat{\mathbf{R}}$, therefore, the simulation time of VAT-MUSIC is in fact a little higher than 75% of that of MUSIC. However, our method has an obvious computational efficiency advantage over the standard MUSIC.

6. Conclusions

We have proposed a novel VAT-MUSIC algorithm by regarding the real-part of the array covariance matrix as an entire array covariance matrix of a virtual array with available sinal model for DOA estimate. VAT-MUSIC involves only real-valued computations with limited spectral search, and hence reduce the complexity by a factor about four. Moreover, VAT-MUSIC has no dependence on array configurations, and it is hence can be used with arbitrary arrays in practice. Simulations show that the proposed algorithm provides an efficient performance-to-complexity tradeoff as compared to the standard MUSIC.

Acknowledgement

This work is supported by National Natural Science Foundation of China (61501142, 61501144), China Postdoctoral Science Foundation (2015M571414) and Natural Science Foundation of Shandong Province (ZR2014FQ003).

Appendix A. Proof of Equation (15)

We begin the proof by using (4) to rewrite $\mathbb{R}$ as

$$\begin{aligned}\mathbb{R} &= \frac{1}{2}\left(\mathbf{R}+\mathbf{R}^*\right)\\ &= \frac{1}{2}\left[\mathbf{A}(\boldsymbol{\Theta})\ \mathbf{A}^*(\boldsymbol{\Theta})\right]\times\begin{bmatrix}\mathbb{R}_s & \mathbf{0}\\ \mathbf{0} & \mathbb{R}_s\end{bmatrix}\\ &\quad\times\begin{bmatrix}\mathbf{A}^H(\boldsymbol{\Theta})\\ \mathbf{A}^T(\boldsymbol{\Theta})\end{bmatrix}+\sigma_n^2\mathbb{I}_M\\ &\triangleq \mathbb{B}(\boldsymbol{\Theta})\mathbb{R}_s^{\text{virtual}}\mathbb{B}^T(\boldsymbol{\Theta})+\sigma_n^2\mathbb{I}_M. \end{aligned}\tag{A.1}$$

Since there are K pairs of symmetrical sources in $\boldsymbol{\Theta}$, we can write

$$\boldsymbol{\Theta}=\left\{\boldsymbol{\Theta}_1,\boldsymbol{\Theta}_2\right\}\tag{A.2}$$

where

$$\boldsymbol{\Theta}_1=\{-\theta_1,\theta_1,-\theta_2,\theta_2,\ldots,-\theta_K,\theta_K\}\tag{A.3a}$$

$$\boldsymbol{\Theta}_2=\{\theta_{2K+1},\theta_{2K+2},\ldots,\theta_L\}.\tag{A.3b}$$

Note for any two DOAs $\theta_1,\theta_2\in\boldsymbol{\Theta}_2$, we have $\theta_1\neq-\theta_2$. Combining $\boldsymbol{\Theta}=\left\{\boldsymbol{\Theta}_1,\boldsymbol{\Theta}_2\right\}$, $\mathbb{B}(\boldsymbol{\Theta})=\frac{1}{\sqrt{2}}\left[\mathbf{A}(\boldsymbol{\Theta})\ \mathbf{A}^*(\boldsymbol{\Theta})\right]$ and $\mathbf{A}^*(\boldsymbol{\Theta}_1)=\mathbf{A}(-\boldsymbol{\Theta}_1)=\mathbf{A}(\boldsymbol{\Theta}_1)$, we have

$$\begin{aligned}\mathbb{B}(\boldsymbol{\Theta}) &= \frac{1}{\sqrt{2}}\left[\mathbf{A}(\boldsymbol{\Theta}_1)\ \mathbf{A}(\boldsymbol{\Theta}_2)\ \mathbf{A}^*(\boldsymbol{\Theta}_1)\ \mathbf{A}^*(\boldsymbol{\Theta}_2)\right]\\ &= \frac{1}{\sqrt{2}}\left[\mathbf{A}(\boldsymbol{\Theta}_1)\ \mathbf{A}(\boldsymbol{\Theta}_2)\ \mathbf{A}(\boldsymbol{\Theta}_1)\ \mathbf{A}^*(\boldsymbol{\Theta}_2)\right].\end{aligned}\tag{A.4}$$

Due to the Vandermonde structure of the array manifold, we have

$$\begin{aligned}\operatorname{rank}\left[\mathbb{B}(\boldsymbol{\Theta})\right] &= \operatorname{rank}\left[\mathbf{A}(\boldsymbol{\Theta}_1)\ \mathbf{A}(\boldsymbol{\Theta}_2)\ \mathbf{A}^*(\boldsymbol{\Theta}_2)\right]\\ &= 2L-K.\end{aligned}\tag{A.5}$$

Because $\mathbb{R}_s^{\text{virtual}}$ is a real diagonal matrix of full rank (since the sources are uncorrelated), we can write $\mathbb{R}_s^{\text{virtual}}\triangleq\mathbb{V}\mathbb{V}^T$, where $\mathbb{V}$ is also a real diagonal matrix of full rank. Therefore, we have

$$\begin{aligned}\operatorname{rank}\left[\mathbb{B}(\boldsymbol{\Theta})\mathbb{R}_s^{\text{virtual}}\mathbb{B}^T(\boldsymbol{\Theta})\right] &= \operatorname{rank}\left\{[\mathbb{B}(\boldsymbol{\Theta})\mathbb{V}][\mathbb{B}(\boldsymbol{\Theta})\mathbb{V}]^T\right\}\\ &= \operatorname{rank}\left[\mathbb{B}(\boldsymbol{\Theta})\mathbb{V}\right]\\ &= \operatorname{rank}\left[\mathbb{B}(\boldsymbol{\Theta})\right]\\ &= 2L-K,\end{aligned}\tag{A.6}$$

which further leads to

$$\mathbb{U}^T\mathbb{B}(\boldsymbol{\Theta})\mathbb{R}_s^{\text{virtual}}\mathbb{B}^T(\boldsymbol{\Theta})\mathbb{U}=\operatorname{diag}\left\{\alpha_1,\alpha_2,\ldots,\alpha_{2L-K},0,\ldots,0\right\}.\tag{A.7}$$

Using (A.7), we have

$$\begin{aligned}\mathbb{U}^T\mathbb{R}\mathbb{U} &= \mathbb{U}^T\mathbb{B}(\boldsymbol{\Theta})\mathbb{R}_s^{\text{virtual}}\mathbb{B}^T(\boldsymbol{\Theta})\mathbb{U}+\sigma_n^2\mathbb{U}^T\mathbb{U}\\ &= \operatorname{diag}\left\{\alpha_1,\alpha_2,\ldots,\alpha_{2L-K},0,\ldots,0\right\}+\sigma_n^2\mathbb{I}\end{aligned}\tag{A.8}$$

which implies that the eigenvalues of $\mathbb{R}$ are

$$\xi_i=\begin{cases}\alpha_i+\sigma_n^2, & i=1,2,\ldots,2L-K\\ \sigma_n^2, & i=2L-K+1,2,\ldots,M\end{cases}\tag{A.9}$$

and the proof is completed.

Appendix B. Proof of Equation (25)

In a noise environment, the virtual noise-free direct-data matrix $\mathbf{X}_{\text{virtual}}$ is perturbed by AGWN as

$$\widehat{\mathbf{X}}_{\text{virtual}}=\mathbf{X}_{\text{virtual}}+\widetilde{\mathbf{N}}=\begin{bmatrix}\widehat{\mathbf{X}} & \widehat{\mathbf{X}}^*\end{bmatrix}\tag{B.1}$$

and its SVD is in fact given by

$$\widehat{\mathbf{X}}_{\text{virtual}} = \widehat{\mathbf{E}}_s\widehat{\mathbf{W}}_s\widehat{\mathbf{F}}_s^H + \widehat{\mathbf{E}}_n\widehat{\mathbf{W}}_n\widehat{\mathbf{F}}_n^H. \tag{B.2}$$

Noting that

$$\begin{aligned}\widehat{\mathbf{X}}_{\text{virtual}}\widehat{\mathbf{X}}_{\text{virtual}}^H &= \begin{bmatrix}\widehat{\mathbf{X}} & \widehat{\mathbf{X}}^*\end{bmatrix}\begin{bmatrix}\widehat{\mathbf{X}}^H(t)\\ \widehat{\mathbf{X}}^T(t)\end{bmatrix}\\ &= 2\text{Re}\left(\widehat{\mathbf{X}}\widehat{\mathbf{X}}^H\right)\\ &= 2N\text{Re}\left(\widehat{\mathbf{R}}\right)\end{aligned} \tag{B.3}$$

we have

$$\widehat{\mathbf{E}}_s\widehat{\mathbf{W}}_s^2\widehat{\mathbf{E}}_s^H + \widehat{\mathbf{E}}_n\widehat{\mathbf{W}}_n^2\widehat{\mathbf{E}}_n^H = \widehat{\mathbb{U}}_s\left(2N\widehat{\mathbb{Q}}_s\right)\widehat{\mathbb{U}}_s^T + \widehat{\mathbb{U}}_n\left(2N\widehat{\mathbb{Q}}_n\right)\widehat{\mathbb{U}}_n^T \tag{B.4}$$

which implies that

$$\widehat{\mathbf{W}}_s^2 = 2N\widehat{\mathbb{Q}}_s, \quad \widehat{\mathbf{E}}_s = \widehat{\mathbb{U}}_s \tag{B.5a}$$

$$\widehat{\mathbf{W}}_n^2 = 2N\widehat{\mathbb{Q}}_n, \quad \widehat{\mathbf{E}}_n = \widehat{\mathbb{U}}_n. \tag{B.5b}$$

Therefore, the perturbation of the noise matrix $\mathbb{U}_n$ equals to the perturbation of $\mathbf{E}_n$. Using (B.5) and lemma 1, it can be easily concluded by comparing (21) with (24) that

$$\begin{aligned}\Delta\mathbb{U}_n &= \Delta\mathbf{E}_n\\ &= -\mathbf{E}_s\mathbf{W}_s^{-1}\mathbf{F}_s^H\widetilde{\mathbf{N}}^H\mathbf{E}_n\\ &= -\mathbf{E}_s\mathbf{W}_s^{-1}\mathbf{F}_s^H\widetilde{\mathbf{N}}^H\mathbb{U}_n\end{aligned} \tag{B.6}$$

which completes the proof.

Appendix C. Proof of Equation (26)

Using (25) and the zero means of AGWN, it can be easily proven with a high SNR assumption that

$$\lim_{N\to\infty}\widehat{\mathbb{U}}_n\widehat{\mathbb{U}}_n^T = \mathbb{U}_n\mathbb{U}_n^T. \tag{C.1}$$

Hence, $f(\theta)$ is a consistent estimate for θ_l [37] [38], and we can obtain the second-order approximation of the derivative of $f(\theta)$ about the true value θ_l as

$$f'(\theta_l) + f''(\theta_l)\left(\widehat{\theta}_l - \theta_l\right) \approx 0 \tag{C.2}$$

where $f'(\theta_l) \triangleq \frac{df(\theta)}{d\theta}$ and $f''(\theta_l) \triangleq \frac{df'(\theta)}{d\theta}$ are the first- and second-order derivatives of $f(\theta)$ with respect to θ_l, respectively, which are given by

$$f'(\theta_l) = 2\mathbb{a}_{\text{re}}^T(\theta_l)\widehat{\mathbb{U}}_n\widehat{\mathbb{U}}_n^T\mathbb{d}_{\text{re}}(\theta_l) + 2\mathbb{a}_{\text{im}}^T(\theta_l)\widehat{\mathbb{U}}_n\widehat{\mathbb{U}}_n^T\mathbb{d}_{\text{im}}(\theta_l) \tag{C.3a}$$

$$f''(\theta_l) = 2\mathbb{d}_{\text{re}}^T(\theta_l)\widehat{\mathbb{U}}_n\widehat{\mathbb{U}}_n^T\mathbb{d}_{\text{re}}(\theta_l) + 2\mathbb{d}_{\text{im}}^T(\theta_l)\widehat{\mathbb{U}}_n\widehat{\mathbb{U}}_n^T\mathbb{d}_{\text{im}}(\theta_l) \tag{C.3b}$$

where the second-order derivatives of $f(\theta)$ is neglected in (C.3b). Substituting (C.3) into (C.2) and performing a straightforward derivation, we can obtain

$$\begin{aligned}\Delta\theta_l &\approx -\frac{f'(\theta_l)}{f''(\theta_l)}\\ &= \frac{\mathbb{a}_{\text{re}}^T(\theta_l)\Delta\mathbb{U}_n\mathbb{U}_n^T\mathbb{d}_{\text{re}}(\theta_l) + \mathbb{a}_{\text{im}}^T(\theta_l)\Delta\mathbb{U}_n\mathbb{U}_n^T\mathbb{d}_{\text{im}}(\theta_l)}{\mathbb{d}_{\text{re}}^T(\theta_l)\mathbb{U}_n\mathbb{U}_n^T\mathbb{d}_{\text{re}}(\theta_l) + \mathbb{d}_{\text{im}}^T(\theta_l)\mathbb{U}_n\mathbb{U}_n^T\mathbb{d}_{\text{im}}(\theta_l)}\end{aligned} \tag{C.4}$$

where $\widehat{\mathbb{U}}_n\widehat{\mathbb{U}}_n^T$ in the denominator of (C.4) is replaced by the true one $\mathbb{U}_n\mathbb{U}_n^T$ without affecting the performance [32] [33] [37] [38]. Inserting (25) into (C.4) gives

$$\Delta\theta_l = \frac{\xi_1 + \xi_2}{m_1 + m_2}. \tag{C.5}$$

where

$$\xi_1 \triangleq \mathbf{p}_1^H\widetilde{\mathbf{N}}^H\mathbb{q}_1$$

$$\xi_2 \triangleq \mathbf{p}_2^H\widetilde{\mathbf{N}}^H\mathbb{q}_2.$$

As $\text{E}[\xi_1] = \text{E}[\xi_2] = 0$ and $\text{E}[\xi_1\xi_2] = \text{E}[\xi_2\xi_1]$, it follows from (C.5) that

$$\begin{aligned}\text{MSE}_{\text{VAT-MUSIC}}\left(\widehat{\theta}_l\right) &\triangleq \text{E}\left[|\Delta\theta_l|^2\right]\\ &= \frac{\text{E}\left[|\xi_1|^2\right] + \text{E}\left[|\xi_2|^2\right] + 2\text{E}[|\xi_1\xi_2|]}{|m_1 + m_2|^2}.\end{aligned} \tag{C.6}$$

Now, consider the first term of (C.6). Expanding $\widetilde{\mathbf{N}}\mathbf{p}_1$ as a weighted sum of the columns of $\widetilde{\mathbf{N}}$ and using (2), we obtain

$$\begin{aligned}\text{E}\left[|\xi_1|^2\right] &= \mathbb{q}_1^T\text{E}\left[\widetilde{\mathbf{N}}\mathbf{p}_1\mathbf{p}_1^H\widetilde{\mathbf{N}}^H\right]\mathbb{q}_1\\ &= \mathbb{q}_1^T\text{E}\left[\sum_i p_{1,i}\widetilde{\mathbf{n}}_i\sum_j p_{1,j}^*\widetilde{\mathbf{n}}_j^H\right]\mathbb{q}_1\\ &= \mathbb{q}_1^T\left[\sum_i\sum_j\left(p_{1,i}p_{1,j}^*\right)\text{E}\left\{\widetilde{\mathbf{n}}_i\widetilde{\mathbf{n}}_j^H\right\}\right]\mathbb{q}_1\\ &= \mathbb{q}_1^T\left[\sum_i\sum_j\left(p_{1,i}p_{1,j}^*\right)\delta(i-j)\sigma_n^2\mathbb{I}_M\right]\mathbb{q}_1\\ &= \sigma_n^2\|\mathbf{p}_1\|^2\|\mathbb{q}_1\|^2.\end{aligned} \tag{C.7}$$

where $p_{1,i}$ and $\mathbf{n}_i$ are the ith element of $\mathbf{p}_1$ and the ith column of $\widetilde{\mathbf{N}}$, respectively. In a similar way, we can obtain the second term of (C.6) as

$$\text{E}\left[|\xi_2|^2\right] = \sigma_n^2\|\mathbf{p}_2\|^2\|\mathbb{q}_2\|^2. \tag{C.8}$$

Expanding $\widetilde{\mathbf{N}}^H\mathbb{q}_1$ and $\widetilde{\mathbf{N}}\mathbf{p}_2$ as weighted sums of the columns of $\widetilde{\mathbf{N}}^H$ and $\widetilde{\mathbf{N}}$, respectively, using (2), we obtain the third term of (C.6) as

$$\begin{aligned}\text{E}[|\xi_1\xi_2|] &= \mathbf{p}_1^H\text{E}\left[\widetilde{\mathbf{N}}^H\mathbb{q}_1\mathbf{p}_2^H\widetilde{\mathbf{N}}^H\right]\mathbb{q}_2\\ &= \mathbf{p}_1^H\text{E}\left[\sum_i q_{1,i}\widetilde{\mathbf{n}}_i^H\sum_j p_{2,j}^*\widetilde{\mathbf{n}}_j^H\right]\mathbb{q}_2\\ &= \mathbf{p}_1^H\left[\sum_i\sum_j\left(q_{1,i}p_{2,j}^*\right)\text{E}\left\{\widetilde{\mathbf{n}}_i^H\widetilde{\mathbf{n}}_j^H\right\}\right]\mathbb{q}_2\\ &= 0\end{aligned} \tag{C.9}$$

where $\widetilde{\mathbf{n}}_i$ is the ith row of $\widetilde{\mathbf{N}}$. Substituting (C.7)~ (C.9) into (C.6), we finally obtain equation (26) and the proof is completed.

References

[1] J. Krim, M. Viberg, Two decades of array signal processing research: the parametric approach, IEEE Signal Process. Mag. 13 (3) (1996) 67–94.

[2] F.G. Yan, M. Jin, S. Liu, X.L. Qiao, Real-valued MUSIC for efficient direction estimation with arbitrary array geometries, IEEE Trans. Signal Process. 62 (6) (2014) 1548–1560.

[3] F.G. Yan, B. Cao, J.J. Rong, Y. Shen, M. Jin, Spatial aliasing for efficient direction-of-arrival estimation based on steering vector reconstruction, EURASIP J. Adv. Signal Process. 121 (2016), doi:10.1186/s13634-016-0419-y.

[4] F.G. Yan, Y. Shen, M. Jin, X.L. Qiao, Computationally efficient direction finding using polynomial rooting with reduced-order and real-valued computations, J Syst. Eng. Electron. 27 (4) (2016b) 739–745.

[5] F.G. Yan, Z.K. Chen, M.J. Sun, Y. Shen, M. Jin, Two-dimensional direction-of-arrivals estimation based on one-dimensional search using rank deficiency principle, Int. J. Antennas Propag. 2015 (2015) 8. Article ID 127621. doi: 10.1155/2015/127621.

[6] F.G. Yan, T. Jin, M. Jin, Y. Shen, Subspace-based direction-of-arrival estimation using centro-symmetrical arrays, Eletron. Lett. 27 (11) (2016) 1895–1896.

[7] Y. Ephraim, N. Merhav, H.L.V. Trees, Min-norm interpretations and consistency of MUSIC, MODE and ML, IEEE Trans. Signal Process. 43 (12) (1995) 2937–2942.

[8] R. Roy, T. Kailath, ESPRIT-estimation of signal parameters via rotational invariance techniques, IEEE Trans. Signal Process. 37 (7) (1989) 984–995.

[9] P. Pelin, A fast minimization technique for subspace fitting with arbitrary array manifolds, IEEE Trans. Signal Process. 49 (12) (2001) 2935–2939.

[10] J.W. Shin, Y.J. Lee, H.N. Kim, Reduced-complexity maximum likelihood direction-of-arrival estimation based on spatial aliasing, IEEE Trans. Signal Process. 62 (24) (2014) 6568–6581.

[11] F.G. Yan, M. Jin, X.L. Qiao, Low-complexity DOA estimation based on compressed MUSIC and its performance analysis, IEEE Trans. Signal Process 61 (8) (2013) 1915–1930.
[12] D.A. Linebarger, R.D. DeGroat, E.M. Dowling, Efficient direction-finding methods employing forward-backward averaging, IEEE Trans. Signal Process. 42 (8) (1994) 2136–2145.
[13] K.C. Huarng, C.C. Yeh, A unitary transformation method for angle-of-arrival estimation, IEEE Trans. Signal Process. 39 (1991) 975–977.
[14] M. Pesavento, A.B. Gershman, M. Haardt, Unitary root-MUSIC with a real-valued eigendecomposition: a theoretical and experimental performance study, IEEE Trans. Signal Process. 48 (5) (2000) 1306–1314.
[15] C. Qian, L. Huang, H.C. So, Improved unitary root-MUSIC for DOA estimation based on pseudo-noise resampling, IEEE Signal Process. Lett 21 (2) (2014) 140–144.
[16] M. Haardt, J.A. Nossek, Unitary ESPRIT: how to obtain increased estimation accuracy with a reduced computational burden, IEEE Trans. Signal Process 43 (5) (1995) 1232–1242.
[17] A.B. Gershman, P. Stoica, On unitary and forward-backward MODE, Digital Signal Process. 9 (2) (1999) 67–75.
[18] N. Yilmazer, J. Koh, T.K. Sarkar, Utilization of a unitary transform for efficient computation in the matrix pencil method to find the direction of arrival, IEEE Trans. Signal Process. 54 (2006) 175–181.
[19] F.G. Yan, Y. Shen, M. Jin, Fast DOA estimation based on a split subspace decomposition on the array covariance matrix, Signal Process. 115 (2015) 1–8.
[20] B. Friedlander, The root-MUSIC algorithm for direction finding with interpolated arrays, Signal Process. 30 (1993) 15–29.
[21] C.P. Mathews, M.D. Zoltowski, Eigenstructure techniques for 2-D angle estimation with uniform circular arrays, IEEE Trans. Signal Process. 42 (9) (1994) 2395–2407.
[22] F. Belloni, A. Richter, V. Koivunen, DoA estimation via manifold separation for arbitrary array structures, IEEE Trans. Signal Process. 55 (10) (2007) 4800–4810.
[23] M. Rbsamen, A.B. Gershman, Direction-of-arrival estimation for nonuniform sensor arrays: from manifold separation to Fourier domain MUSIC methods, IEEE Trans. Signal Process. 57 (2009) 588–599.
[24] P. Hyberg, M. Jansson, B. Ottersten, Array interpolation and bias reduction, IEEE Trans. Signal Process. 52 (10) (2004) 2711–2720.
[25] P. Hyberg, M. Jansson, B. Ottersten, Array interpolation and DOA MSE reduction, IEEE Trans. Signal Process 53 (12) (2005) 4464–4471.
[26] J. Zhuang, W. Li, A. Manikas, Fast root-MUSIC for arbitrary arrays, Electron.Lett. 46 (2) (2010).
[27] J.W. Shin, Y.J. Lee, H.N. Kim, Reduced-complexity maximum likelihood direction-of-arrival estimation based on spatial aliasing, IEEE Trans. Signal Process. 62 (24) (2014) 6568–6581.
[28] K.C. Tan, Z. Goh, A detailed derivation of arrays free of higher rank ambiguities, IEEE Trans. Signal Process 44 (2) (1996) 351–359.
[29] G.H. Golub, C.H.V. Loan, Matrix computations, Baltimore, MD: The Johns Hopkins University Press, 1996.
[30] V. Vasylyshyn, Improving the performance of root-MUSIC via pseudo-noise resampling and conventional beamformer, in: 2011 Conference on Microwaves, Radar and Remote Sensing Symposium(MRRS)., 8, 2011, pp. 309–312.
[31] Xu, Kailath, Fast subspace decomposition, IEEE Trans. Signal Process. 42 (3) (1994) 539–551.
[32] F. Li, H. Liu, R.J. Vaccaro, Performance analysis for DOA estimation algorithms: unification, simplification, and observations, IEEE Trans. Aerosp. Electron. Syst. 29 (4) (1993).
[33] F. Li, R.J. Vaccaaro, Analysis of min-norm and MUSIC with arbitrary array geometry, IEEE Trans. Aerosp. Electron. Syst. 26 (6) (1990) 976–985.
[34] C. Chambers, T.C. Tozer, K.C. Sharman, S.D. Tariq, Temporal and spatial sampling influence on the estimates of superimposed narrowband signals: When less can mean more, IEEE Trans. Signal Process. 44 (12) (2004) 3085–3098.
[35] P. Pal, P.P. Vaidyanathan, Nested arrays: a novel approach to array processing with enhanced degrees of freedom, IEEE Trans. Signal Process. 58 (8) (2010) 4167–4181.
[36] F.G. Yan, M. Jin, X.L. Qiao, Source localization based on symmetrical MUSIC and its statistical performance analysis, Sci. China Inf. Sci. 56 (6) (2013) 1–13.
[37] P. Stoica, K.C. Sharman, Maximum likelihood methods for direction-of-arrival estimation, IEEE Trans. Acoust. Speech Signal Process. 38 (7) (1990) 1132–1143.
[38] J. Xin, A. Sano, Computationally efficient subspace-based method for direction-of-arrival estimation without eigendecomposition, IEEE Trans. Signal Process. 52 (4) (2004) 876–893.